

# Designing thermal energy harvesting devices with natural materials through optimized microstructures

Qingxiang Ji<sup>a,b</sup>, Xueyan Chen<sup>a,b</sup>, Jun Liang<sup>c</sup>, Vincent Laude<sup>b</sup>, Sébastien Guenneau<sup>d</sup>, Guodong Fang<sup>a,\*</sup>, Muamer Kadic<sup>b</sup>

<sup>a</sup> National Key Laboratory of Science and Technology on Advanced Composites in Special Environments, Harbin Institute of Technology, Harbin, 150001, China

<sup>b</sup> Institute FEMTO-ST, CNRS, University Bourgogne Franche-Comté, 25000 Besançon, France

<sup>c</sup> Institute of Advanced Structure Technology, Beijing Institute of Technology, Beijing 100081, China

<sup>d</sup> UMI 2004 Abraham de Moivre-CNRS, Imperial College, London SW7 2AZ, UK

---

## Abstract

Metamaterial thermal energy devices obtained from transformation optics have recently attracted wide attention due to their vast potential in energy storage, thermal harvesting or heat manipulation. However, these devices usually require inhomogeneous and extreme material parameters which are difficult to realize in large-scale applications. Here, we demonstrate a general process to design thermal harvesting devices with available natural materials through optimized composite microstructures. **We first design a cross-shaped microstructure and apply two-scale homogenization theory to obtain its effective properties.** Optimal Latin hypercube technique, combined with a genetic algorithm, is then implemented on the microstructure to achieve optimized geometrical parameters. The optimized microstructure can accurately approximate the behavior of transformed materials. We design such devices and numerically characterize good **thermal energy harvesting performances.** **To validate the wide application range of our approach, we illustrate other types of microstructures like split rings and rectangles, and show that they mimic well the required constitutive parameters.** The approach we propose can be used to design novel thermal harvesting devices available with existing technology, and can also act as a beneficial vehicle to explore other transformation optics enabled designs.

**Keywords:** Transformation thermodynamics; Thermal energy harvesting; Microstructures; Optimization

---

## 1. Introduction

Transformation optics was first proposed to perform cloaking on electromagnetic waves, based on form-invariance of the governing equations after coordinates transformation [1]. Since then the concept was promoted in various physical fields [2–7], creating miscellaneous devices, like invisible cloaks [8], carpets [9], invisible sensors [10], illusion devices [11–13] or hyperlenses [14, 15]. Transformation thermodynamics, a counterpart of transformation-optics, has been proposed to guide heat flux in thermal manipulation and generate novel thermal meta-

devices, such as heat cloaks, thermal energy harvesting devices, thermal sensors, etc [16–24]. Thermal energy harvesting devices, which can focus and harvest ambient thermal energy without severe perturbations to the heat profile outside the devices, have vast potential in improving the energy-conversion efficiency of existing technologies [25].

A challenge for thermal meta-devices is that they often require inhomogeneous and anisotropic constitutive parameters which are difficult to realize especially for large-scale applications. As the heterogeneous constitutive profile is position-dependent and continuous, some form of discretization is required. Moreover, anisotropic materials can be ap-

---

<sup>1</sup>fanggd@hit.edu.cn

proximated by structures of thin and alternating layers based on effective medium theory [26]. Thermal devices following this principle were fabricated and experimentally characterized [21, 27]. In these works, step-wise approximation of the ideal parameters were made, which sacrificed the performances to reduce fabrication difficulty. Other researchers realized thermal meta-devices with bulk isotropic materials using the scattering-cancellation approach [28–32]. Following this approach, a class of solar-shaped thermal harvesting devices were demonstrated, which could manipulate and concentrate the heat flux using natural materials without singularities [33, 34]. However, these meta-devices are always shaped as regular profiles (cylinder, sphere or ellipse), as the scattering-cancellation method is non-trivial for irregular or complex shapes. In some works, topology optimization method is applied to design thermal meta-devices, where the optimized structures always occupy irregular shapes that impose high requirements on **fabrication** [35–37].

Except for the mentioned strategies, do we have methods that can both offer good performance and fabrication simplicity? The answer is positive. Researchers [38, 39] demonstrated that the constitutive medium can be approximated by microstructures in the context of acoustic metamaterials. Thanks to similarities between the governing equations for acoustic and thermal fields, a similar approach can be implemented for thermal metamaterials. Then the key problem is to determine the effective property of the built microstructure and find the proper parameters of the microstructure to mimic desired transformed parameters. Ji *et al.* [40] achieved thermal concentration using fiber reinforced microstructures based on simplified effective medium theory. Pomot *et al.* [41] realized acoustic cloaking by microstructures with several types of perforations, combined with a genetic algorithm. We note that the partial differential equations (PDEs) therein have the same structure to the heat equation in the static limit, in which case one simply has to replace the density by the conductivity and all the asymptotic analysis carries through. Moreover, PDEs in Ref. [41] are supplied with homogeneous Neumann boundary conditions that stand for rigid walls in acoustics, and insulating walls in thermodynamics. It is thus tempting

to implement homogenization and effective medium theories similar to those already used in acoustic metamaterials, however bearing in mind that in the dynamic regime the acoustic wave (elliptic) PDE and the heat diffusion (parabolic) PDE are very different in nature.

In our work we focus on the thermal field and establish a general design road map to obtain realizable thermal harvesting devices utilizing microstructures. We apply two-scale homogenization theory to determine the equivalent thermal properties and employ the Optimal Latin-Hypercube technique to obtain desired design parameters. Beyond this problem, the process is applicable to other microstructures and to wave problems (such as in acoustics). We stress that because of their complexity, the microstructures we investigate here would be challenging to achieve otherwise. Finally we numerically characterize such thermal harvesting devices with natural materials and verify their harvesting efficiency by finite element simulations.

## 2. Methods

### 2.1. Concept design

We recall the heat conduction equation without heat sources

$$\nabla \cdot (k\nabla T) - \rho c \frac{\partial T}{\partial t} = 0, \quad (1)$$

where  $\nabla$  is the gradient,  $T$  is the temperature,  $\rho c$  is the product of density by heat capacity and  $k$  denotes the heat conductivity. Following the theory of transformation optics [1] and thermodynamics [4], the governing equation will remain unchanged under a coordinate transformation when the transformed parameters satisfy

$$k' = \frac{JkJ^T}{\det(J)} \quad \text{and} \quad (\rho c)' = \frac{\rho c}{\det(J)}, \quad (2)$$

where  $J = \frac{\partial(x',y',z')}{\partial(x,y,z)}$  is the **Jacobian of the geometric transformation from  $(x, y, z)$  to  $(x', y', z')$  coordinates (i.e. from virtual to physical space)**,  $J^T$  its transpose and  $\det(J)$  its determinant. We first consider steady-state case where parameters  $\rho c$  vanish. The transformed conductivity  $k'$  derived by Eq. (2) is usually

anisotropic and **position** dependent, which is difficult to achieve in practice. To remove the singularities and make the proposed device simpler to realize, we choose the following nonlinear transformation that maps **virtual space**  $\Omega(r)$  onto **physical space**  $\Omega'(r')$ :

$$r' = r_2 \left( \frac{r}{r_2} \right)^C, \quad (3)$$

which yields constant radial ( $k'_r$ ) and tangential heat conductivity ( $k'_\theta$ ) in cylindrical coordinates as

$$\frac{k'_r}{k_b} = C \quad \text{and} \quad \frac{k'_\theta}{k_b} = \frac{1}{C}, \quad (4)$$

where  $k_b$  denotes **thermal conductivity of the background medium** and  $C$  is a constant with  $C > 1$ . Here,  $r_1$  and  $r_2$  are the inner radius and the outer radius of the designed shell region, respectively (see details in the supplemental material).

In stark contrast to the material parameters obtained from rigorous linear transformation, such a device is homogeneous in materials composition and its performance is only determined by the thermal-conduction anisotropy (characterized by constant  $C$ ; see details in the supplemental material). We employ this geometric transformation as it avoids the need for extreme spatially-varying parameters and thus the transformed medium will be much easier to implement in practice. Moreover, it is enough for the proof-of-concept demonstration. We stress that the method we describe is indeed also applicable to the design of **more complex** transformation-based thermal devices.

For clarity, we outline the design process for the general case with a specific example. Assume that we create a cylindrically symmetric thermal harvesting device with inner radius  $r_1 = 0.01$  m and outer radius  $r_2 = 0.04$  m (see Fig. 1). The proposed device can harvest thermal energy from the surroundings and concentrate it into the inner domain  $r' < r_1$ . Heat energy density in the inner domain is thus significantly increased. In our design, the thermal conductivity of the background is  $k_b = 132 \text{ Wm}^{-1}\text{K}^{-1}$ . We set  $C = 2$ , which implies that for the shell region we have  $k'_r = 264 \text{ Wm}^{-1}\text{K}^{-1}$  and  $k'_\theta = 66 \text{ Wm}^{-1}\text{K}^{-1}$ . Now we turn to the realization of shell region parameters by two natural materials  $A$  and  $B$  through optimized microstructures.

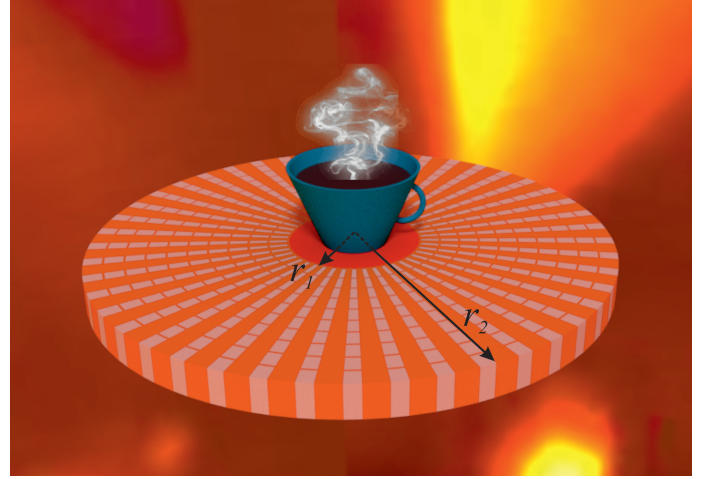


**Fig. 1.** Schematic representation of a possible realization of the thermal harvesting device. The shell displays some periodicity along the azimuthal direction, which is a hallmark of a concentrator. Such a device can harvest thermal energy from its surroundings. Heat flows are concentrated into the inner domain  $r' < r_1$  thanks to the designed shell region  $r_1 \leq r' \leq r_2$ .

## 2.2. Homogenization of the heat conduction equation

The material distributions in Eq. (4) need to be mapped onto a microstructure exhibiting prescribed constitutive parameters. We build a medium with identical elementary cells repeating periodically in space (see Fig. 2). Generally, the well-established effective medium theory plays a **prominent** role in determining effective properties and is easy and direct for simple geometries. When designing meta-devices with complex-shaped structures, however, it would be far from trivial to evaluate the equivalent properties. Here we apply instead two-scale homogenization theory [42] to determine effective parameters with an asymptotic approach.

We consider a two-dimensional periodic medium with square elementary cells  $[0, \eta]^2$  of side-length  $\eta \ll 1$ . The solution  $T_\eta$  of the steady-state heat equation with fast oscillating parameters  $A_\eta = k(x/\eta, y/\eta)$

$$\nabla \cdot (k_\eta \nabla T_\eta) = 0 \quad (5)$$

two-scale converges [43], when  $\eta$  tends to zero, to the solution  $T_{\text{hom}}$  of the homogenized heat equation

$$\nabla \cdot (k_{\text{hom}} \nabla T_{\text{hom}}) = 0. \quad (6)$$

The effective property of the periodic medium is

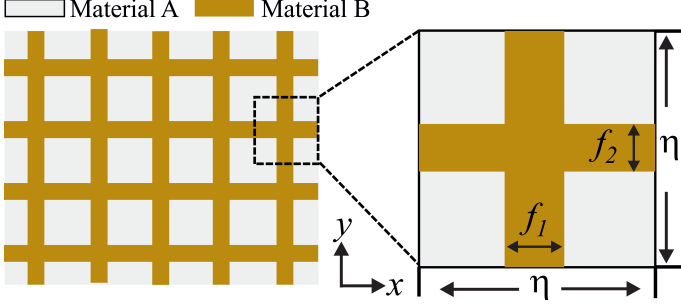


**Fig. 2.** Schematic illustration of 2D periodic lattices defined by 2 parameters (area fractions  $f_1$  and  $f_2$ ). We choose this microstructure to mimic the desired medium of the shell region through homogenization and optimization.

given by

$$k_{\text{hom}} = \begin{bmatrix} \langle k \rangle - \langle k \partial_x V_1 \rangle & -\langle k \partial_x V_2 \rangle \\ -\langle k \partial_y V_1 \rangle & \langle k \rangle - \langle k \partial_y V_2 \rangle \end{bmatrix}, \quad (7)$$

where  $\partial_x := \partial/\partial x$ ,  $\partial_y := \partial/\partial y$  and  $\langle \cdot \rangle$  denotes the mean operator over the periodic cell.  $V_1(x, y)$  and  $V_2(x, y)$  are solutions defined up to an additive constant of auxiliary problems of thermostatic type on the periodic cell [42]:

$$\begin{cases} \nabla \cdot [k(x, y) \nabla (V_1 - x)] = 0 \\ \nabla \cdot [k(x, y) \nabla (V_2 - y)] = 0 \end{cases}. \quad (8)$$

We solve the auxiliary problems in weak form by using COMSOL Multiphysics, which sets up the finite element problem with periodic conditions imposed to the field on opposite ends of the elementary cell. We note in passing  $V_1$  and  $V_2$  are unique solutions of Eq. (8) up to additive constants, but these constants do not affect the homogenized conductivity, as one can see that in Eq. (7) only the partial derivatives of  $V_1$  and  $V_2$  are involved. The potentials  $V_1(x, y)$  and  $V_2(x, y)$  of an illustrative case ( $f_1 = 0.6576, f_2 = 0.0835$ ) are shown in Fig. 3, where we obtain the effective conductivity as

$$k_{\text{hom}} = \begin{bmatrix} 66.01 & 3.3 \cdot 10^{-11} \\ -1.2 \cdot 10^{-11} & 263.97 \end{bmatrix} \approx \begin{bmatrix} k_1 & \\ & k_2 \end{bmatrix}. \quad (9)$$

It is noticed that in Eq. (9) the off-diagonal components are almost negligible and originate from numerical errors. The resulting spurious artificial anisotropy can be safely ignored. We emphasize

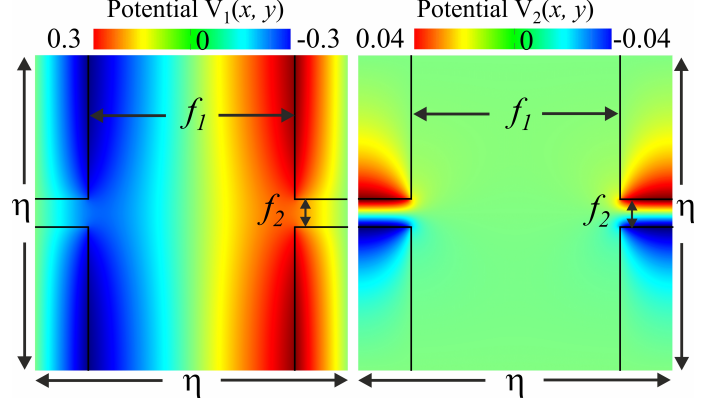


**Fig. 3.** Potentials  $V_1(x, y)$  and  $V_2(x, y)$  of the illustrative case where  $f_1 = 0.6576, f_2 = 0.0835$ .

that with the finite element method, the effective tensor can be obtained for any periodic composite and that the same technique was implemented before in acoustics [41] and electromagnetism [42], in which case the effective density and permittivity tensors **respectively** can be deduced from the same annex problems as in our thermal case.

The effective properties of the medium can be tuned by several design parameters such as **geometrical** (here we use area fractions  $f_1$  and  $f_2$ ) and material properties (thermal conductivities  $k_A$  and  $k_B$ ). We restrict our attention here to predefined material properties and set the geometrical parameters as variables. Our goal is to find the set of geometrical parameters which properly mimic the homogenized medium. Therefore, the geometry of elementary cells should be tuned to obtain desired equivalent properties. Considering the heavy workload of the trial-and-error method, we implement an Optimal Latin hypercube technique to solve the problem. We note here that the two-scale homogenization technique has been already used to design a thermal concentrator similar to the one shown in Fig. 1 and to show that a concentrator consisting of concentric layers would require some complex valued conductivities with sign-shifting imaginary parts [44]. In the present case, we investigate doubly periodic designs and thus we do not face such pitfalls.

### 2.3. Optimal Latin Hypercube Design

Optimal Latin Hypercube Sampling (OLHS) technique is applied to optimize the spatial positions of control points. The aim of this process is to design

a matrix where the sample points spread as evenly as possible within the design region. This method is efficient and robust due to its enhanced stochastic evolutionary algorithm and significant reduction in matrix calculations to evaluate new/modified designs during searching [45]. In this work, we pre-define the two materials as air ( $k_A = 0.026$ ) and copper ( $k_B = 400$ ) in units of  $\text{Wm}^{-1}\text{K}^{-1}$  and select the geometrical (area fraction) parameters  $f_1$  and  $f_2$  as design variables. The ranges of these variables are defined as  $0.5 < f_1 < 0.8$  and  $0.05 < f_2 < 0.1$  after initial estimation. We generate one hundred sample points by OLHS technique, and calculate corresponding effective thermal conductivity of the periodic medium for each sample point using the two-scale homogenization theory. Details of the generated sample points and calculated results are listed in Table S1. We emphasize the importance of choosing proper ranges of the variables. If, for instance, we use much larger ranges for  $f_1$  and  $f_2$ , the derived values can be less accurate unless a more refined discretization (more sample points) is chosen.

We then create an approximation surrogate model from the obtained one hundred space samples [46]. The surrogate model is built by the Elliptical Basis Function Neural Network technique which establishes a relation between design targets ( $k_1$  and  $k_2$ ) and variables ( $f_1$  and  $f_2$ ), as shown in Fig. 4 (a-b). We use two estimators to evaluate the reliability of the surrogate model, the coefficient of determination ( $R^2$ ) and the root mean square error (RMSE). These are defined as

$$R^2 = 1 - \frac{\sum_{i=1}^m (y_i - \hat{y}_i)^2}{\sum_{i=1}^m (y_i - \bar{y})^2}, \quad (10)$$

$$\text{RMSE} = \sqrt{\frac{\sum_{i=1}^m (y_i - \hat{y}_i)^2}{m}}, \quad (11)$$

where  $y_i$  and  $\hat{y}_i$  are respectively the real value and the predicted value of the objective function over the same sample points,  $\bar{y}$  is the mean value of all objective functions and  $m$  is the total number of sampling points. The closer  $R^2$  is to 1 and RMSE is to 0, the more accurate the model. In Fig. 4 (c-d), we can observe that the predicted values (values obtained by the surrogate model) are in good agreement with the actual values (values on the sample points).

The calculated  $R^2$  and RMSE are listed in Table 1. The average error and the maximum error among all samples are also shown. In the constructed surrogate models,  $R^2$  is larger than 0.99997 and RMSE are smaller than 0.00012. The maximum error remains close to 0, which demonstrates that the **surrogate model is accurate**.

**Table 1**

Accuracy of the constructed surrogate model.

Error type	$k_1$	$k_2$
RMSE	$1.2 \cdot 10^{-3}$	$4.88 \cdot 10^{-5}$
Average	$6.45 \cdot 10^{-4}$	$3.52 \cdot 10^{-5}$
Maximum	$5.47 \cdot 10^{-3}$	$1.88 \cdot 10^{-4}$
$R^2$	0.99997	1

Now we proceed with the inverse homogenization problem, that is, we want to find the particular set of design parameters which best mimic the transformed medium [47]. The optimization problem amounts to minimizing the objective function:

$$E(k_1, k_2, \alpha, \beta) = \alpha |k_1 - k'_r| + \beta |k_2 - k'_\theta|, \quad (12)$$

where  $\alpha$  and  $\beta$  are **positive** weighting factors for the two objective sub-functions such that  $\alpha + \beta = 1$ . The function  $E(k_1, k_2, \alpha, \beta)$  measures the overall difference between obtained and objective values. We define  $\alpha = \beta = 0.5$ , i.e. equal weights for the diagonal tensor elements  $k_1$  and  $k_2$ . The principle is to obtain a global minimum within the discrete solution space. We solve this inverse problem by using a Non-Dominated Sorting Genetic Algorithm approach [48]. The one hundred random structures, corresponding to the parameter space samples obtained by the OLHS method, form the first generation. During the search process, the population size and the number of generations are defined as 12 and 200, respectively. New generations are created using crossover and mutation processes. We set the mutation distribution index and crossover distribution index as 20 and 10, respectively. The crossover probability is set as 0.9. For the sake of clarity, we do not detail the well-established genetic algorithm approach. In short, the Non-Dominated Sorting Genetic Algorithm performs well enough in our case and enables us to determine efficiently the desired design parameters.

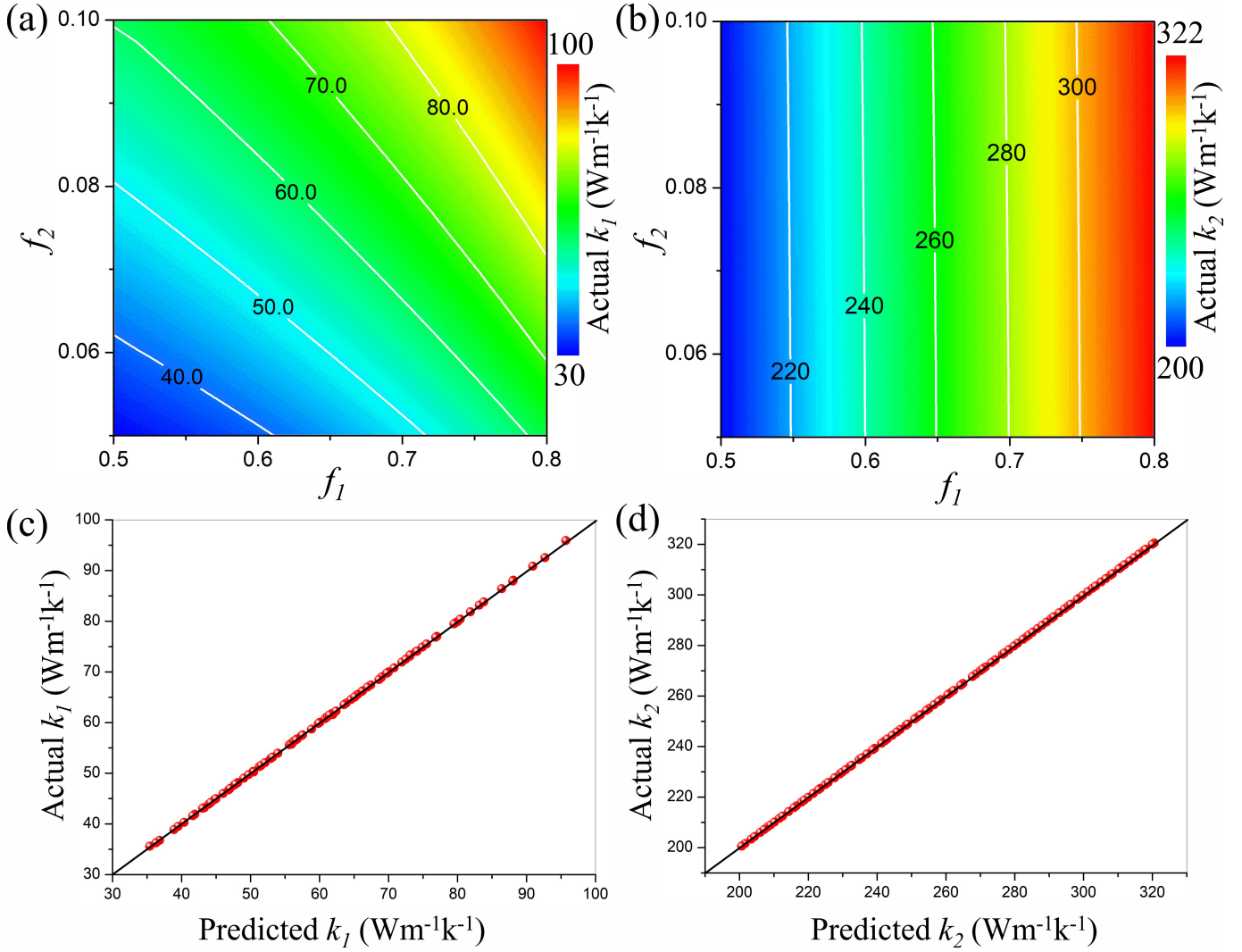


**Fig. 4.** Panels (a) and (b) show the relation between design targets (heat conductivities  $k_1$  and  $k_2$ ) and design variables (geometrical parameters  $f_1$  and  $f_2$ ). The results are obtained basing on the chosen sample points and using two-scale homogenization theory. Panels (c) and (d) show good agreement between actual values and predicted values of the heat conductivities, demonstrating the reliability of the surrogate model. The indices  $k_1$  and  $k_2$  denote heat conductivity of the elementary cell in the x and y directions, respectively.

Following this approach, we obtain the desired set of parameters as  $f_1 = 0.6576$  and  $f_2 = 0.0835$  for  $C = 2$ . We then implement the microstructure and calculate the corresponding heat conductivities. The result are listed in Table.2. It can be seen that the obtained parameters closely mimic the desired transformed medium.

### 3. Scheme validation and discussion

#### 3.1. Recipe for experimental realization

We now turn to the theoretical recipe for realizing thermal harvesting based on optimized composite microstructures. Note that the heat conductivity

**Table 2**

Comparison of predicted value and targeted value for the derived set of parameters.

	Predicted	Targeted	Relative difference
$k_1(\text{Wm}^{-1}\text{K}^{-1})$	263.97	264	0.01%
$k_2(\text{Wm}^{-1}\text{K}^{-1})$	66.01	66	0.02%

in Eq. (4) is expressed in  $(r, \theta)$  polar coordinates while the microstructure is designed in  $(x, y)$  Cartesian coordinates. To build a cylindrical thermal harvesting device, we discretize the shell region into numerous units and transplant microstructures with

matched geometrical parameters into each unit. We design in this paper a discrete thermal harvesting device with 15 radial layers and 45 tangential sectors. Similarly to what has been done in Ref. [41], we could have considered an increasing number of layers and sectors to very accurately approximate the idealized thermal concentrator parameters. However, we focus here on a practically implementable design. The materials constituting the microstructure are naturally available materials: copper (material A) and air (material B). It is understood that the device could be built from other materials. We use copper and air here considering their applicability for realistic experiments.

Numerical calculations were conducted, where temperatures at the left and right boundary are respectively imposed as 1 K and 0 K, for easiness in normalization. We apply Neumann (perfect insulator) conditions at other boundaries. As indicated in the scheme (Fig. 5), iso-thermal lines are significantly compressed to the inner domain ( $r \leq r_1$ ). Hence, heat flux density in the inner domain is enlarged, implying that more heat energy is concentrated into the central region. In addition, iso-thermal lines in the background are uniform with little perturbations. That is, the heat energy is harvested and concentrated into the central region without much perturbation of the external thermal field. We emphasize that similar computations would also hold for time-harmonic acoustic and electromagnetic equations.

We further conduct a quantitative analysis of the thermal harvesting behavior of the proposed scheme. Two measurement lines are defined. An horizontal line ( $y = 0$ ) is selected to reveal perturbations of the external thermal field whereas a vertical line ( $x = r_2$ ) is chosen to illustrate the heat harvesting efficiency, as shown in Fig. 6. We also build an additional contrast plate that occupies the same area as the harvesting device but that is composed only of a homogeneous background medium. The following index  $\eta$  is defined to evaluate the energy harvesting efficiency as

$$\eta = \left| \frac{T_{x=r_1} - T_{x=-r_1}}{T_{x=r_2} - T_{x=-r_2}} \right|. \quad (13)$$

An index  $M_V$  is introduced to characterize the pertur-

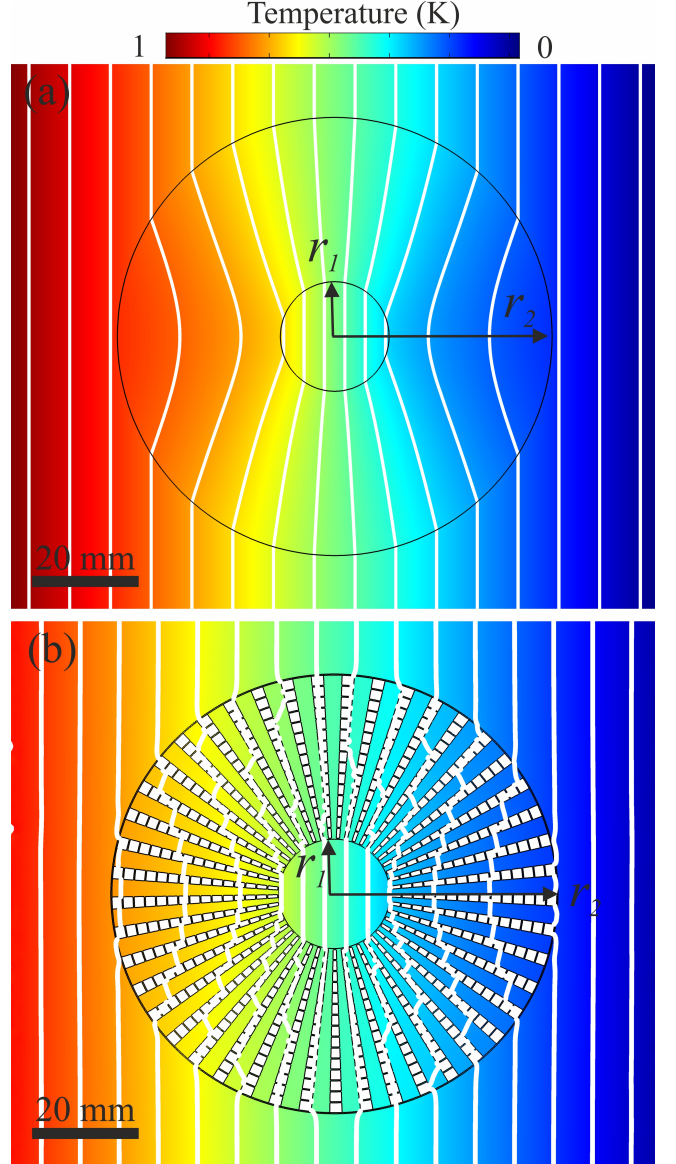


**Fig. 5.** Temperature fields in the steady state for (a) the ideal case and (b) the proposed thermal harvesting device. In both cases, heat flows are concentrated to the inner domain without much perturbations to the external thermal field.

bations to external fields (*i.e.* the thermal neutrality of the concentrator)

$$M_V = \frac{\int_{\Omega} |T(x, y, z) - T_r(x, y, z)| d\Omega}{\int_{\Omega} d\Omega}, \quad (14)$$

where  $\Omega$  denotes the probe domain of external thermal fields and  $T_r$  represents the temperature field of the homogeneous medium. The index  $M_V$  reveals all perturbations to the external heat profile [49].

It is apparent in Fig. 6(a) that thermal energy is significantly concentrated into the inner domain, as

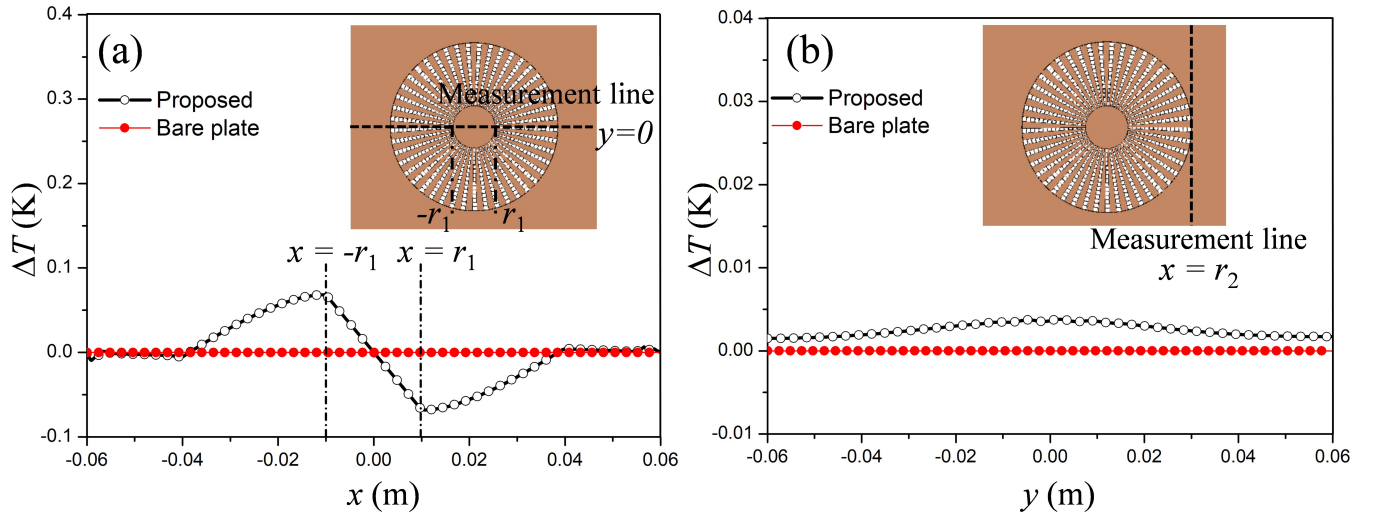


**Fig. 6.** Comparison of temperature profiles between the harvesting device and the contrast plate along the measurement lines (a)  $y = 0$  and (b)  $x = r_2$ . All results are obtained in the steady-state and the insets denote positions of measurement lines. We define  $\Delta T = |T(x, y, z) - T_r(x, y, z)|$  to quantitatively demonstrate the heat harvesting performances. Significant heat-focusing in the inner domain ( $-r_1 < x < r_1$ ) and minor fluctuations in external domain (along  $x = r_2$ ) are both observed, demonstrating good heat concentrating performances.

a tight focusing with a local heat-intensity increase is observed. We list thermal gradients inside the inner domain (characterized by  $\Delta T_{in} = |T_{x=r_1} - T_{x=-r_1}|$ ) and harvesting efficiencies for different cases in Tab. 3. The results indicate that thermal gradients in the central region are almost twice as large as in the contrast plate. The concentration efficiency is significantly lifted. Both results reach nearly theoretical values, demonstrating that the heat concentrating scheme is both effective and accurate.

**Table 3**

Thermal harvesting performances for different cases.

Index	Ideal	Proposed	Bare plate
$\Delta T_{in}$ (K)	0.4	0.39	0.2
$\eta$	0.5	0.49	0.25
$M_V$ (K)	0	0.0025	0.0003

It can be observed in Fig. 6(b) that temperatures along the vertical measurement line are almost uniform, indicating that the external thermal field is only slightly influenced. We notice some minor perturbations in Tab. 3 which are mainly due to the discretization process and to numerical errors.

Thus far, all that has been achieved for heat can be directly translated to airborne acoustics (with rigid inclusions) and electromagnetism (with per-

fectly conducting inclusions, in the case when the magnetic field is polarized perpendicular to the  $xy$ -plane), since governing equations are identical in the static limit, and so results in Fig. 6 and 7 hold for the acoustic and electromagnetic counterparts of the thermal concentrator. We would like to investigate now the diffusive nature of heat conduction. We define same boundary conditions as the steady state case and focus here on the evolution of thermal harvesting performance over time. Temperature distributions at different time steps  $t$  are shown in Fig. (7), where thermal gradients and perturbations are also plotted as a function of time. It is observed that perturbations of the external thermal profile increase and then decrease after a certain lapse of time, whereas the thermal gradient of the object increases gradually toward its maximum value. Generally, the proposed design performs well for harvesting thermal energy, with significant heat flux concentrated in the inner domain and little perturbation to the outside thermal field, once the permanent regime has been reached. We stress that the design process proves feasible as the created device works efficiently and converges to almost the same harvesting performance as in the ideal case.

The heat concentration efficiency is directly determined by the constant  $C$  [34], which in turn can be



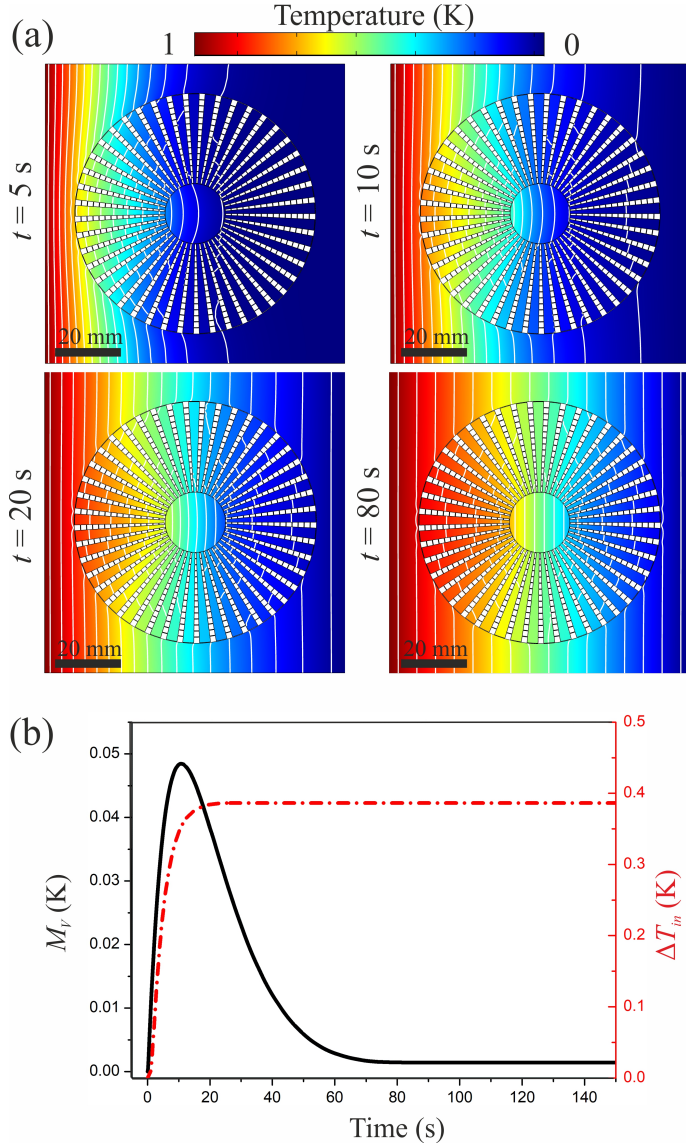


**Fig. 7.** Thermal harvesting performances of the concentrator in the transient regime. (a) Temperature fields are illustrated at different times  $t$ . The performances get gradually better after a certain lapse of time. (b) Thermal gradients of the inner domain ( $\Delta T_{in} = |T_{x=r_1} - T_{x=-r_1}|$ ) and perturbations to external thermal field ( $M_V$ ) are plotted as functions of time. The quantitative results agree well with those revealed in (a).

approached by the material properties and the geometry of the microstructures. To gain more insights into the underlying mechanism of the microstructure, we derive and show in Fig. 8 the relation between design variables (area fraction  $f_1$  and  $f_2$ ) and the heat concentration efficiency. For comparison, we further assume two other materials C and D to substitute for material B, with heat conductivity  $k_C < k_B < k_D$ . It is observed that higher concentration efficiency re-

quires larger  $f_1$  and smaller  $f_2$  which directly indicates larger geometrical anisotropy. Besides, we notice that smaller design variables are needed to achieve a given efficiency for a larger conductivity of the second material (for constant material A). Larger material anisotropy also allows for a larger maximum concentration efficiency.

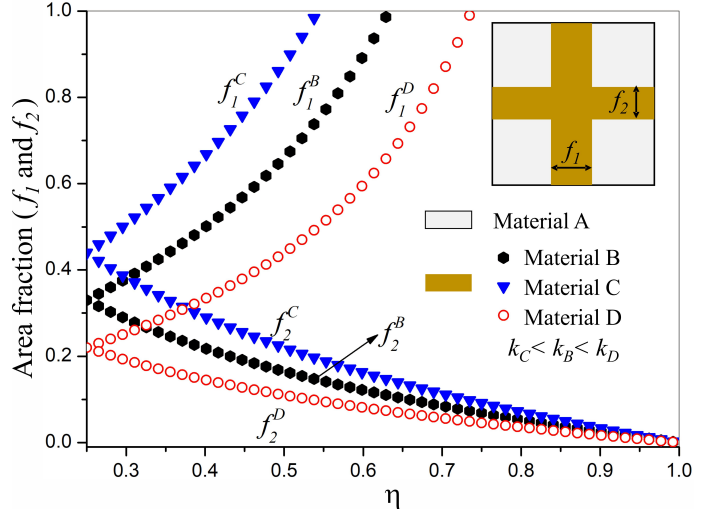


**Fig. 8.** Relation between design variables (area fractions  $f_1$  and  $f_2$ ) and the concentration efficiency. The inset shows the studied elementary cell where one material is pre-defined as  $k_A = 0$  and another material is varied. In addition to material B ( $k_B = 400 \text{ Wm}^{-1}\text{K}^{-1}$ ), we also considered material C ( $k_C = 300 \text{ Wm}^{-1}\text{K}^{-1}$ ) and material D ( $k_D = 600 \text{ Wm}^{-1}\text{K}^{-1}$ ) for a comparison.

### 3.2. Additional microstructures

Note that the microstructure we employed in Fig. 2 is not the unique choice. One can use other elementary cells as long as they are appropriate to obtain the required anisotropy. To validate the wide-range application of our approach, we further present several other elementary cells and build corresponding devices. Steady state simulations are conducted with same boundaries with the aforementioned case. In Fig. 9(a), we set material properties as design variables and recover the widely used solar-shaped device. In Fig. 9(b), we obtain the same design as in Fig. 1 but based on a different elementary cell obtained by a sub-lattice translation. Besides, we show in Fig. 9(c) a split ring element cell for which it seems unlikely that the effective medium theory could be easily applied. Good harvesting performance is again achieved without much perturbations

to the external field. As a note, the symmetry of the split ring element cell is reduced compared to the other cases, but the effective tensor remains diagonal. The strength of our approach becomes apparent when dealing with such more complex geometries, where the application of effective medium theory is far from trivial.

We stress that using the optimization approach in this paper high-performance thermal-harvesting designs can be obtained that meet given external constraints, such as maximum or minimum values for material properties and geometrical parameters. We can search for the best solution among materials properties, microstructures and geometrical parameters within the full available range, providing a substantial flexibility and many degrees of freedom in practical applications.

We considered in this paper two-dimensional (2D) harvesting devices as fabrication and measurement are presumably simpler than in 3D. The proposed optimization method, however, is also well suited to the design of 3D thermal harvesting devices. A major difference is that more design variables are required in 3D, and thus more computational resources would be required to undertake such a study, for which the theoretical part of the present work would apply *mutatis mutandis*.

#### 4. Conclusion

We proposed a general method to design thermal-energy harvesting devices from naturally available materials. We designed composite microstructures and calculated their effective conductivity by the two-scale homogenization technique. We then implemented the Optimal Latin hypercube method to obtain design parameters that can best mimic the transformed medium. We built a harvesting device model based on the obtained optimized microstructures and demonstrated good thermal harvesting performance, thereby validating the effectiveness of our design method.

The optimization method adds great flexibility to the constraints that can be imposed on devices, which allows one to find the best possible solutions with different geometrical structures and component materials. We stress that the flexibility and simplicity of

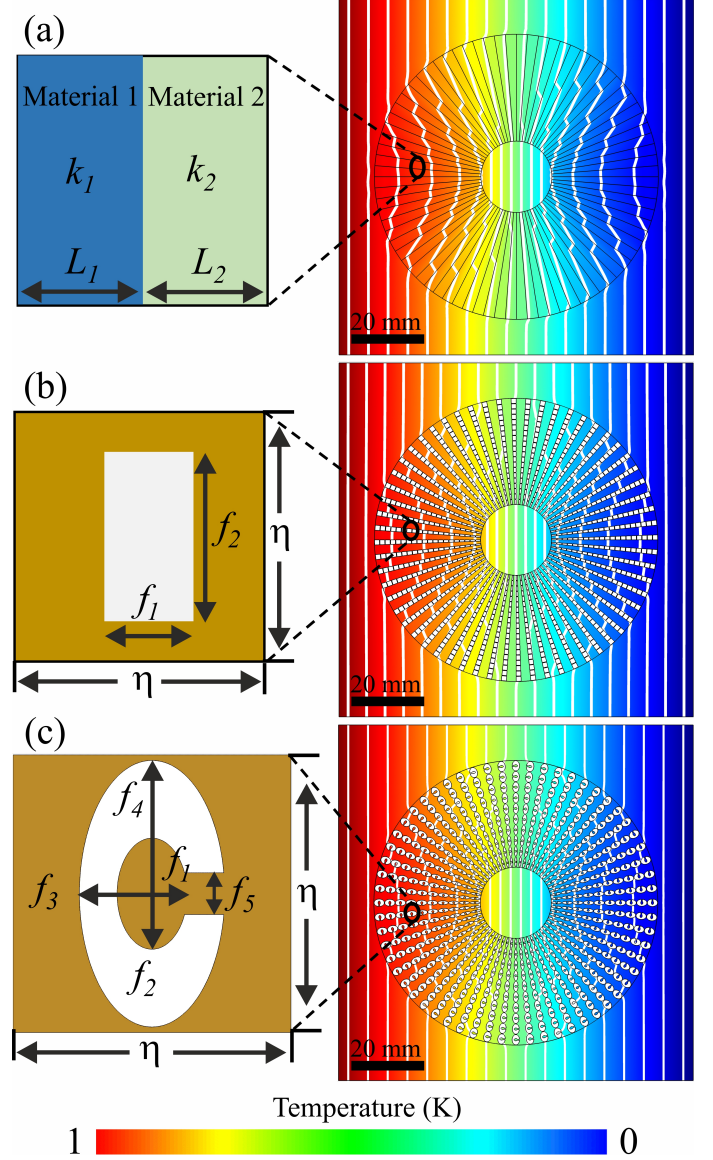


**Fig. 9.** Additional optimized microstructures and corresponding thermal harvesting performance. (a) Laminar structures defined by two material parameters ( $k_1$  and  $k_2$ ) if  $L_1 = L_2$  and two additional geometrical parameters if  $L_1 \neq L_2$ . The optimized parameters are  $k_1 = 0.26782$  and  $k_2 = 3.7328$  if we impose  $L_1 = L_2$ . (b) Elementary cell defined by two geometrical parameters  $f_1 = 0.34238$ ,  $f_2 = 0.91675$ . (c) Split ring structure defined by five geometrical parameters. The optimized parameters are  $f_1 = 0.1037$ ,  $f_2 = 0.1261$ ,  $f_3 = 0.4799$ ,  $f_4 = 0.2614$ , and  $f_5 = 0.0994$ . In panels (b,c) the materials used are the same as those in Fig. 2. Following the proposed design process, we have considered different microstructures and have obtained the same thermal conductivities, i.e.  $k'_r = 264 \text{ Wm}^{-1}\text{K}^{-1}$  and  $k'_\theta = 66 \text{ Wm}^{-1}\text{K}^{-1}$ .

the method is a good addition to existing heat manipulation techniques, including other thermal functionalities, i.e. cloaking and illusion. It also paves a path

for novel optical, acoustic and electromagnetic devices based on form-invariant governing equations.

## Acknowledgments

This work was supported by the EIPHI Graduate School [grant number ANR-17-EURE-0002]; the French Investissements d’Avenir program, project ISITEBFC [grant number ANR-15-IDEX-03]; and the National Natural Science Foundation of China [grant numbers 11732002 and 11672089].

## References

- [1] J. B. Pendry, D. Schurig, D. R. Smith, Controlling electromagnetic fields, *Science* 312 (5781) (2006) 1780–1782.
- [2] R. Schittny, M. Kadic, T. Bückmann, M. Wegener, Invisibility cloaking in a diffusive light scattering medium, *Science* 345 (6195) (2014) 427–429.
- [3] T. Bückmann, M. Thiel, M. Kadic, R. Schittny, M. Wegener, An elasto-mechanical unfeelability cloak made of pentamode metamaterials, *Nature Communications* 5 (2014) 4130.
- [4] S. Guenneau, C. Amra, D. Veynante, Transformation thermodynamics: cloaking and concentrating heat flux, *Optics Express* 20 (7) (2012) 8207–8218.
- [5] Y. Achaoui, A. Diatta, M. Kadic, S. Guenneau, Cloaking in-plane elastic waves with swiss rolls, *Materials* 13 (2) (2020) 449.
- [6] M. Kadic, M. Wegener, A. Nicolet, F. Zolla, S. Guenneau, A. Diatta, Elastodynamic behavior of mechanical cloaks designed by direct lattice transformations, *Wave Motion* 92 (2020) 102419.
- [7] M. Kadic, S. Guenneau, S. Enoch, S. A. Ramakrishna, Plasmonic space folding: Focusing surface plasmons via negative refraction in complementary media, *ACS nano* 5 (9) (2011) 6819–6825.
- [8] M. Farhat, S. Guenneau, S. Enoch, Ultrabroadband elastic cloaking in thin plates, *Physical Review Letters* 103 (2) (2009) 024301.
- [9] J. Li, J. B. Pendry, Hiding under the carpet: a new strategy for cloaking, *Physical Review Letters* 101 (20) (2008) 203901.
- [10] T. Yang, X. Bai, D. Gao, L. Wu, B. Li, J. T. Thong, C.-W. Qiu, Invisible sensors: Simultaneous sensing and camouflaging in multiphysical fields, *Advanced Materials* 27 (47) (2015) 7752–7758.
- [11] M. Liu, Z. Lei Mei, X. Ma, T. J. Cui, Dc illusion and its experimental verification, *Applied Physics Letters* 101 (5) (2012) 051905.
- [12] R. Hu, S. Zhou, Y. Li, D.-Y. Lei, X. Luo, C.-W. Qiu, Illusion thermotics, *Advanced Materials* 30 (22) (2018) 1707237.
- [13] S. Zhou, R. Hu, X. Luo, Thermal illusion with twinborn-like heat signatures, *International Journal of Heat and Mass Transfer* 127 (2018) 607–613.
- [14] Z. Liu, H. Lee, Y. Xiong, C. Sun, X. Zhang, Far-field optical hyperlens magnifying sub-diffraction-limited objects, *Science* 315 (5819) (2007) 1686–1686.
- [15] J. Li, L. Fok, X. Yin, G. Bartal, X. Zhang, Experimental demonstration of an acoustic magnifying hyperlens, *Nature Materials* 8 (12) (2009) 931–934.
- [16] C. Fan, Y. Gao, J. Huang, Shaped graded materials with an apparent negative thermal conductivity, *Applied Physics Letters* 92 (25) (2008) 251907.
- [17] X. Shen, J. Huang, Thermally hiding an object inside a cloak with feeling, *International Journal of Heat and Mass Transfer* 78 (2014) 1–6.
- [18] L. Xu, J. Huang, Controlling thermal waves with transformation complex thermotics, *International Journal of Heat and Mass Transfer* 159 (2020) 120133.
- [19] J. Qin, W. Luo, P. Yang, B. Wang, T. Deng, T. Han, Experimental demonstration of irregular thermal carpet cloaks with natural bulk material, *International Journal of Heat and Mass Transfer* 141 (2019) 487–490.
- [20] Y. Liu, W. Guo, T. Han, Arbitrarily polygonal transient thermal cloaks with natural bulk materials in bilayer configurations, *International Journal of Heat and Mass Transfer* 115 (2017) 1–5.
- [21] R. Schittny, M. Kadic, S. Guenneau, M. Wegener, Experiments on transformation thermodynamics: molding the flow of heat, *Physical Review Letters* 110 (19) (2013) 195901.
- [22] T. Han, X. Bai, J. T. Thong, B. Li, C.-W. Qiu, Full control and manipulation of heat signatures: Cloaking, camouflage and thermal metamaterials, *Advanced Materials* 26 (11) (2014) 1731–1734.
- [23] X. Peng, R. Hu, Three-dimensional illusion thermotics with separated thermal illusions, *ES Energy & Environment* 6 (2019) 39–44.
- [24] S. Huang, J. Zhang, M. Wang, R. Hu, X. Luo, Macroscale thermal diode-like black box with high transient rectification ratio, *ES Energy & Environment* 6 (2019) 51–6.
- [25] G. Xu, H. Zhang, Y. Jin, Achieving arbitrarily polygonal thermal harvesting devices with homogeneous parameters through linear mapping function, *Energy Conversion and Management* 165 (2018) 253–262.
- [26] D. Schurig, J. Mock, B. Justice, S. A. Cummer, J. B. Pendry, A. Starr, D. R. Smith, Metamaterial electromagnetic cloak at microwave frequencies, *Science* 314 (5801) (2006) 977–980.
- [27] S. Narayana, Y. Sato, Heat flux manipulation with engineered thermal materials, *Physical Review Letters* 108 (21) (2012) 214303.
- [28] T. Han, X. Bai, D. Gao, J. T. Thong, B. Li, C.-W. Qiu, Experimental demonstration of a bilayer thermal cloak, *Physical Review Letters* 112 (5) (2014) 054302.
- [29] X. Zhang, X. He, L. Wu, Ellipsoidal bifunctional thermal-electric transparent device, *Composite Structures* 234

- (2020) 111717.
- [30] H. Xu, X. Shi, F. Gao, H. Sun, B. Zhang, Ultrathin three-dimensional thermal cloak, *Physical Review Letters* 112 (5) (2014) 054301.
- [31] T. Han, P. Yang, Y. Li, D. Lei, B. Li, K. Hippalgaonkar, C.-W. Qiu, Full-parameter omnidirectional thermal metadevices of anisotropic geometry, *Advanced Materials* 30 (49) (2018) 1804019.
- [32] G. Xu, X. Zhou, J. Zhang, Bilayer thermal harvesters for concentrating temperature distribution, *International Journal of Heat and Mass Transfer* 142 (2019) 118434.
- [33] F. Chen, D. Y. Lei, Experimental realization of extreme heat flux concentration with easy-to-make thermal metamaterials, *Scientific Reports* 5 (2015) 11552.
- [34] T. Han, J. Zhao, T. Yuan, D. Y. Lei, B. Li, C.-W. Qiu, Theoretical realization of an ultra-efficient thermal-energy harvesting cell made of natural materials, *Energy & Environmental Science* 6 (12) (2013) 3537–3541.
- [35] G. Fujii, Y. Akimoto, Topology-optimized thermal carpet cloak expressed by an immersed-boundary level-set method via a covariance matrix adaptation evolution strategy, *International Journal of Heat and Mass Transfer* 137 (2019) 1312–1322.
- [36] G. Fujii, Y. Akimoto, Cloaking a concentrator in thermal conduction via topology optimization, *International Journal of Heat and Mass Transfer* 159 (2020) 120082.
- [37] G. V. Alekseev, D. A. Tereshko, Particle swarm optimization-based algorithms for solving inverse problems of designing thermal cloaking and shielding devices, *International Journal of Heat and Mass Transfer* 135 (2019) 1269–1277.
- [38] J. Mei, Z. Liu, W. Wen, P. Sheng, Effective dynamic mass density of composites, *Physical Review B* 76 (13) (2007) 134205.
- [39] D. Torrent, J. Sánchez-Dehesa, Acoustic cloaking in two dimensions: a feasible approach, *New Journal of Physics* 10 (6) (2008) 063015.
- [40] Q. Ji, G. Fang, J. Liang, Achieving thermal concentration based on fiber reinforced composite microstructures design, *Journal of Physics D: Applied Physics* 51 (31) (2018) 315304.
- [41] L. Pomot, C. Payan, M. Remillieux, S. Guenneau, Acoustic cloaking: Geometric transform, homogenization and a genetic algorithm, *Wave Motion* 92 (2020) 102413.
- [42] F. Zolla, S. Guenneau, Artificial ferro-magnetic anisotropy: homogenization of 3d finite photonic crystals, in: *IUTAM Symposium on Asymptotics, Singularities and Homogenisation in Problems of Mechanics*, Springer, 2003, pp. 375–384.
- [43] G. Allaire, Homogenization and two-scale convergence, *SIAM Journal on Mathematical Analysis* 23 (6) (1992) 1482–1518.
- [44] D. Petiteau, S. Guenneau, M. Bellieud, M. Zerrad, C. Amra, Thermal concentrator homogenized with solar-shaped mantle, *arXiv preprint arXiv:1508.05081* (2015).
- [45] J.-S. Park, Optimal latin-hypercube designs for computer experiments, *Journal of Statistical Planning and Inference* 39 (1) (1994) 95–111.
- [46] M.-W. Mak, S.-Y. Kung, Estimation of elliptical basis function parameters by the em algorithm with application to speaker verification, *IEEE Transactions on Neural Networks* 11 (4) (2000) 961–969.
- [47] E. Cherkaev, Inverse homogenization for evaluation of effective properties of a mixture, *Inverse Problems* 17 (4) (2001) 1203.
- [48] K. Deb, A. Pratap, S. Agarwal, T. Meyarivan, A fast and elitist multiobjective genetic algorithm: Nsga-ii, *IEEE Transactions on Evolutionary Computation* 6 (2) (2002) 182–197.
- [49] Q. Ji, X. Chen, G. Fang, J. Liang, X. Yan, V. Laude, M. Kadic, Thermal cloaking of complex objects with the neutral inclusion and the coordinate transformation methods, *AIP Advances* 9 (4) (2019) 045029.